JOURNAL OF GEOPHYSICAL RESEARCH, VOL. 110, A12S25, doi:10.1029/2005JA011141, 2005

Correction published 16 February 2007

Energy transport in the thermosphere during the solar storms of April 2002

Martin G. Mlynczak,[1] F. Javier Martin-Torres,[2] Geoff Crowley,[3] David P. Kratz,[1] Bernd Funke,[4] Gang Lu,[5] Manuel Lopez-Puertas,[4] James M. Russell III,[6] Janet Kozyra,[7] Chris Mertens,[1] Ramesh Sharma,[8] Larry Gordley,[9] Richard Picard,[8] Jeremy Winick,[8] and Larry Paxton[10]

Received 17 March 2005; revised 18 August 2005; accepted 13 September 2005; published 15 December 2005.

[1] The dramatic solar storm events of April 2002 deposited a large amount of energy into the Earth's upper atmosphere, substantially altering the thermal structure, the chemical composition, the dynamics, and the radiative environment. We examine the flow of energy within the thermosphere during this storm period from the perspective of infrared radiation transport and heat conduction. Observations from the SABER instrument on the TIMED satellite are coupled with computations based on the ASPEN thermospheric general circulation model to assess the energy flow. The dominant radiative response is associated with dramatically enhanced infrared emission from nitric oxide at 5.3 μm from which a total of $\sim 7.7 \times 10^{23}$ ergs of energy are radiated during the storm. Energy loss rates due to NO emission exceed 2200 Kelvin per day. In contrast, energy loss from carbon dioxide emission at 15 μm is only ~2.3% that of nitric oxide. Atomic oxygen emission at 63 μm is essentially constant during the storm. Energy loss from molecular heat conduction may be as large as 3.8% of the NO emission. These results confirm the ''natural thermostat'' effect of nitric oxide emission as the primary mechanism by which storm energy is lost from the thermosphere below 210 km.

Citation: Mlynczak, M. G., et al. (2005), Energy transport in the thermosphere during the solar storms of April 2002, *J. Geophys. Res.*, *110*, A12S25, doi:10.1029/2005JA011141.

1. Introduction

[2] In mid-April 2002, a dramatic series of flares and three associated coronal mass ejections (CMEs) from the Sun impacted the terrestrial environment and substantially altered the thermal structure, chemical composition, dynamics, and radiative environment of the Earth's upper atmosphere. These effects were driven by the deposition of energy from solar particles accelerated in the flare and at shocks traveling through interplanetary space, as well as from magnetic activity triggered by the interaction between the Earth's magnetosphere and the fast CMEs. The fast CMEs piled up the solar wind ahead of them creating shocks and sheath regions. Large double-peaked magnetic storms developed on 17–18 April and 19–20 April. The first peak in each storm was due to the sheath region and the second to the CME itself. The third CME only struck Earth a glancing blow on 23 April producing very mild magnetic activity. The polar cap was filled with energetic solar protons and electrons for much of 7 days, starting from 17 April until well into 24 April. An intensification of the high-energy solar particle events at Earth occurred following an X1.5 class flare on 21 April during an interval of low magnetic activity.

[3] The effects of these events on the neutral thermosphere were observed by the Thermosphere-Ionosphere-Mesosphere Energetics and Dynamics (TIMED) satellite. In particular, increases by factors of as much as 6 to 10 in the rate of infrared emission from nitric oxide (NO) at 5.3 μm were observed by the Sounding of the Atmosphere using Broadband Emission Radiometry (SABER) instrument on the TIMED satellite. Initial analyses of these observations [*Mlynczak et al.*, 2003] led to the development of the concept that NO emission acts as a ''natural thermostat'' allowing the atmosphere to rapidly shed energy through radiation and thereby recover from the effects of a solar or geomagnetic storm on a relatively short timescale.

[4] In this paper we conduct a detailed analysis of the radiative and conductive mechanisms by which storm energy is transported out of the thermosphere. We use a combination of observations of infrared emission made by the SABER instrument on the TIMED satellite and compu-

[1]Science Directorate, NASA Langley Research Center, Hampton, Virginia, USA.
[2]AS & M Inc., Hampton, Virginia, USA.
[3]Southwest Research Institute, San Antonio, Texas, USA.
[4]Instituto de Astrofisica de Andalucia, Granada, Spain.
[5]National Center for Atmospheric Research, Boulder, Colorado, USA.
[6]Hampton University, Hampton, Virginia, USA.
[7]University of Michigan, Ann Arbor, Michigan, USA.
[8]Air Force Research Laboratory, Hanscom Air Force Base, Massachusetts, USA.
[9]G & A Technical Software, Newport News, Virginia, USA.
[10]Johns Hopkins Applied Physics Laboratory, Laurel, Maryland, USA.

0148-0227/05/2005JA011141

Table 1. SABER Channels, Target Species, Measured Spectral Bandpass, and Science Focus

Channel	Target Species	Bandpass, cm^{-1}	Primary Science Focus
1	CO_2	639–698	temperature; cooling rates
2	CO_2	580–763	temperature; cooling rates
3	CO_2	579–763	temperature, cooling rates
4	O_3	1013–1146	ozone; solar heating
5	H_2O	1368–1567	water vapor
6	NO	1863–1945	cooling rates
7	CO_2	2303–2392	carbon dioxide abundance
8	OH	4509–5157	chemical heating; H, O density
9	OH	5741–6416	chemical heating; H, O density
10	O_2	7703–7971	ozone daytime; solar heating; O

tations based on simulations of the atmospheric composition by the ASPEN general circulation model. We assess the total energy radiated from the thermosphere by infrared emission and investigate the energy lost from the thermosphere by heat conduction. Our results based on SABER observations indicate that substantially enhanced emission by NO is the dominant infrared response, followed by modest carbon dioxide (CO_2) emission at 15 μm. Energy loss rates due to NO emission during the storm exceed 2200 Kelvin per day near 52°S latitude. Storm-enhanced emission from CO_2 is found to be only 2.3% that of NO. On the basis of results from the ASPEN general circulation model, we predict essentially no infrared radiative response due to emission by atomic oxygen (O) at 63 μm. We also find a small increase in the rate of molecular heat conduction out of the thermosphere during the storm. The results confirm that nitric oxide truly acts as a ''natural thermostat'' in the terrestrial thermosphere, providing the primary mechanism for storm energy to be rapidly lost from the atmosphere via infrared emission. We note that the response and recovery of the thermosphere to geomagnetic storms has been studied previously [*Maeda et al.*, 1992; *Killeen et al.*, 1997] with the relative importance of radiation and heat conduction assessed by model computations. Our results here are first-time observations of the primary radiative components which can ultimately be used to assess model physics.

[5] In section 2 we discuss the SABER observations and the ASPEN general circulation model. In section 3 we discuss the derivation of the energy emitted by NO from the SABER limb radiance observations. The radiative effects of CO_2 and O are discussed in sections 4 and 5, respectively. Heat conduction is discussed in section 6. A preliminary discussion of the mechanisms responsible for the enhancement of the NO emission is given in section 7. The paper concludes with a summary and recommendations in section 8.

2. SABER Observations and the ASPEN Model

2.1. SABER Instrument

[6] The SABER instrument is a 10 channel limb-scanning radiometer flying on the NASA TIMED satellite. The instrument is described by *Russell et al.* [1999]. The primary objective of SABER is to quantify the thermal structure and energy balance of the mesosphere and lower thermosphere [*Mlynczak*, 1995, 1997]. SABER scans the Earth's limb from 400 km tangent height to a height equivalent to 20 km below the hard Earth surface, simultaneously recording profiles of radiance (W cm^{-2} sr^{-1}) in its 10 spectral channels. The time required for a single SABER scan is 53 s, during which time the spacecraft travels about 350 km or approximately 3 degrees in latitude. The instrument continuously scans the Earth limb in this mode, recording approximately 1600 profiles of limb radiance in each of its 10 channels each day. The SABER scan approach ensures that any infrared emissions from the atmosphere below 400 km falling within the spectral bandpasses will be observed if the signal is larger than the measurement noise. Listed in Table 1 are relevant parameters for each of the 10 SABER channels including target emitting species, spectral bandpass, and primary science focus. The spectral coverage of the instrument is from 1.27 to 15.4 μm.

[7] During the solar storm events of April 2002, SABER observed significant radiance enhancements in the thermosphere at wavelengths of 5.3 μm, 1.27 μm, 4.3 μm, 15 μm, and 2.0 μm. Shown in Figure 1 are single radiance profiles in these channels taken prior to the storm on 14 April 2002 and during the height of the storm on 19 April 2002. The enhancements at 1.27 and 2.0 μm extend to altitudes at which the radiances during quiescent times are within the measurement noise. The enhancements at 2.0 μm are quite interesting as this channel nominally observes the 9–7 and 8–6 bands of the OH molecule in the mesopause region (80–100 km). While it is quite likely that the enhancements at 15, 5.3, 4.3, and 1.27 μm are due to the target molecules for those channels (CO_2, NO, CO_2, and O_2), it is unlikely that the emission in the thermosphere at 150 km is due to highly vibrationally excited Meinel OH bands. A candidate suggestion would be the Noxon ($b^1\Sigma_g - a^1\Delta_g$) band of O_2. However, the spectroscopy of this band [*Fink et al.*, 1986] indicates only a few of its weak lines fall within the spectral bandpass of this SABER channel. The origin of radiation at 2.0 μm is as yet unexplained.

[8] From a perspective of energy flow, clearly the most significant observed radiative enhancement is in the emission at 5.3 μm. Emission from the NO molecule is known to be the major radiative cooling mechanism of the thermosphere above about 115 km [*Kockarts*, 1980]. The dramatic increases in NO emission observed on a short timescale (1 day) by SABER have confirmed a fundamental role is played by NO emission in ameliorating the effects of the storm, i.e., the thermostat effect. The observations also indicate that CO_2 emission at 15 μm also responds to the storm effects and must be investigated for its contribution to the overall thermostat effect. The SABER observations will

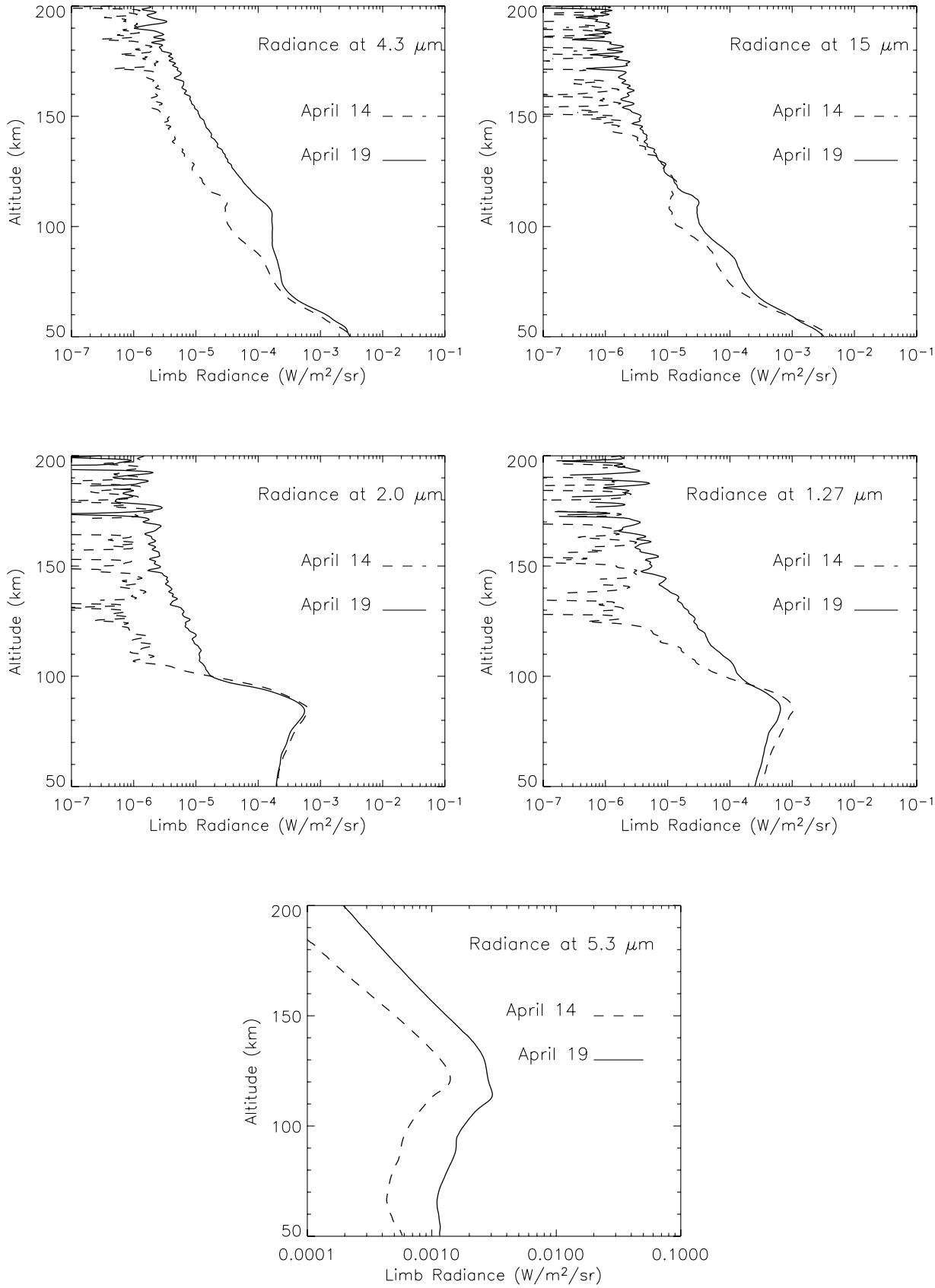

Figure 1. SABER limb radiance profiles at 4.3 μm, 15 μm, 2.0 μm, 1.27 μm, and 5.3 μm on 14 April prior to the onset of the storm (dashed lines) and on 19 April during the storm period.

be complemented by model analyses of emission from atomic oxygen and of energy loss due to heat conduction. We now discuss briefly the ASPEN general circulation model and then continue with a detailed analysis of the SABER observations of the NO and CO_2 emissions.

2.2. ASPEN Model

[9] The model used here is the National Center for Atmospheric Research (NCAR) Thermosphere Ionosphere Mesosphere Electrodynamics General Circulation Model (TIME-GCM), which has been ported to the Southwest Research Institute in San Antonio, Texas where it runs on a Beowulf computer system [*Crowley et al.*, 1999] and is known as the ASPEN model. The TIME-GCM was described by *Roble and Ridley* [1994] and is the latest in a series of three-dimensional (3-D) models developed at NCAR. The ASPEN model is commensurate with the current version of the TIME-GCM in most respects. The inputs required by the model include the solar flux at 57 key wavelengths, auroral particle precipitation, high-latitude electric fields, and tides propagating up from below the 10 hPa (10 mb) lower boundary. There are many ways to specify these inputs to the model. For simplicity, with the diurnally reproducible runs presented here, the inputs to the model include solar flux parameterized using a fixed $F_{10.7}$ index of 75, which represents typical solar minimum conditions. The storm-time model runs are described in detail by G. Crowley et al. (Space weather effects of the April 16–23, 2002, magnetic storm, manuscript in preparation for *Journal of Geophysical Research*, 2005a). Briefly, the size of the auroral oval and the particle characteristics are driven by the *Roble and Ridley* [1987] model, using Hemispheric Power measured approximately every 45 min by the NOAA satellites. The high-latitude electric field distribution is represented using the *Heelis et al.* [1982] model with IMF B_Y measured by the ACE satellite and cross-cap potential estimated from the *Weimer* [1996] empirical model driven by solar wind inputs. The upward propagating tides are forced at the lower boundary of the model using seasonal tidal amplitudes and phases derived from the Global Scale Wave Model (GSWM) of *Hagan et al.* [1999]. The model is also forced by gravity waves propagating from below. This version of the model uses the same gravity wave drag formulation and latitude dependence as the Garcia-Solomon 2-D model [*Garcia et al.*, 1992; *Garcia and Solomon*, 1994]. The gravity waves add directly to the energy budget and the momentum budget and also indirectly via the eddy diffusion terms. The TIME-GCM has been described in detail by *Roble* [1995]. The energy equation solved by the model and the individual energy terms are discussed by G. Crowley et al. (A theoretical study of the energetics of the mesosphere and thermosphere: 1. Solar minimum conditions, manuscript in preparation for Journal of Geophysical Research, 2005b).

3. Analysis of SABER Observations

[10] We conduct analysis of the SABER observations that will lead from the measured SABER limb radiance within the spectral bandpass of the instrument at 5.3 μm to an estimate of the total energy emitted by nitric oxide during the storm period. There are several steps in this process which will be discussed in detail. They are, in order, (1) retrieval of the vertical profile of the rate of emission of energy by the NO molecule (energy per unit volume per unit time) for all emitting bands of NO, not just the fraction observed within the SABER bandpass; (2) the computation of the radiative flux (energy per unit area) exiting the thermosphere for each computed vertical profile of energy loss rate; (3) spatial integration of the fluxes to achieve estimates of instantaneous radiated power (energy per time); (4) assessment of temporal variations followed by meridional and temporal integration to compute the total radiated energy locally and globally. These are now described in detail below in sections 3.1 through 3.4.

3.1. Retrieval of the Volume Emission Rate of Energy

[11] In order to analyze the SABER NO emission measurements in terms of energy loss, we must first derive the local rate of emission from the NO molecule as a function of altitude. The quantity that we wish to derive is the volume emission rate of energy E, energy per unit volume per unit time, typically erg cm^{-3} s^{-1}. These are derived from the SABER limb radiance measurements.

[12] SABER observes emission from the vibration-rotation bands of NO. As a diatomic molecule, NO has one normal mode of vibration. The fundamental ($\upsilon = 1$ to $\upsilon = 0$) band of NO is centered at 1876 cm^{-1} or 5.3 μm. SABER is also sensitive to emission from the 2–1 and 3–2 bands of NO [*Mlynczak et al.*, 2003]. Under quiescent nighttime conditions the dominant emitting band of NO is the 1–0 band, excited by collisions with atomic oxygen. During daytime conditions, and under storm conditions, the higher-lying bands of NO may become important. These are excited by two exothermic chemical reactions between nitrogen atoms and molecular oxygen,

$$\text{(R1)} \qquad N(^4S) + O_2 \rightarrow NO(\upsilon) + O$$

$$\text{(R2)} \qquad N(^2D) + O_2 \rightarrow NO(\upsilon) + O.$$

Thermospheric NO infrared emission, including the emissions from high-lying states excited by these reactions, is discussed by *Dothe et al.* [2002], *Funke and Lopez-Puertas* [2000], and *Sharma et al.* [1998].

[13] SABER measures the infrared limb radiance emitted by NO in a spectral bandpass defined primarily by the interference filter within the optical train of the instrument. The radiative transfer equation describing the SABER measurements is given by

$$R(z_o) = \int_{\nu} \int_{x} J(\nu, x) \frac{\partial \tau(\nu, x)}{\partial x} \varphi(\nu) dx\, d\nu. \qquad (1)$$

$R(z_o)$ is the measured limb radiance (erg cm^{-2} sr^{-1} s^{-1}) at tangent altitude z_o, $J(\nu, x)$ is the source function for infrared emission at wave number ν at point x along the line of sight, $\tau(\nu, x)$ is the transmittance of the atmosphere at wave number ν between point x and the satellite, $\partial\tau(\nu, x)/\partial x$ is the gradient of the transmittance at point x, and $\varphi(\nu)$ is the SABER relative spectral response function.

[14] Fundamental to the interpretation of the SABER data is the assumption that the NO emission from the atmosphere

and observed by SABER is in the weak-line limit of radiative transfer. In the weak line limit, absorption by NO (i.e., self-absorption) is minimal along the line of sight. In this limit, all radiation emitted by the atmosphere in the direction of the instrument escapes the atmosphere and is detected. The radiative transfer equation in the weak line limit is written as

$$R(z_o) = \frac{hc}{4\pi} \sum_{j=1}^{m} \sum_{i=1}^{k} V_{ij}\ \nu_i\ \varphi_i\ dx_j. \tag{2}$$

V_{ij} is the photon volume emission rate (photons cm^{-3} s^{-1}) for ith spectral line in the jth layer of atmosphere along the line of sight, h is Planck's constant, ν_i is the central wave number of the ith line, and c is the speed of light. The summations are taken over all spectral lines of NO (total number equal to k) and over all atmospheric layers (total number equal to m) along the line of sight at tangent altitude z_o. In the weak line limit the emission is independent of spectral line shape.

[15] To evaluate the validity of the weak line limit of radiative transfer in NO for the limb view of SABER, we computed the limb radiance for the NO fundamental band during storm conditions and elevated NO amounts. The radiance was computed using equation (1) with the spectral response function set to 1.0 at all wave numbers. We also computed the radiance with equation (1) but with the transmittance computation in the weak line limit, i.e., $\tau_\nu = 1 - k_\nu * u$, where k_ν is the absorption cross section and u is the optical mass. The radiances agreed to better than 3% between 210 km and 100 km tangent height, the limits of this study. We conclude from this that the assumption of weak line radiative transfer is valid for these analyses.

[16] With the validity of the weak line limit of radiative transfer established, we now move to invert the radiative transfer equation to derive the volume emission rates. Equation (2) can readily be written as a matrix equation of the form $Ae = r$, where A is a triangular matrix containing the path lengths dx_j, e is a vector of volumetric emission rates of energy (erg cm^{-3} s^{-1}) to be determined, and r is a vector of measured SABER limb radiances. This matrix equation is directly inverted by virtue of being a triangular matrix. Upon inversion, the elements e_j of vector e are given by

$$\mathrm{e}_j = hc \sum_{i=1}^{k} V_{ij}\nu_i\varphi_i. \tag{3}$$

An individual element e_j is the volume emission of NO at altitude j which includes all i spectral lines of NO as weighted by the spectral response function φ of the instrument.

[17] In order to estimate the total energy radiated by the NO molecule, we must determine the total emission rate E_j at altitude j. We must adjust the elements e_j to account for the effects of the spectral response of the instrument and must also include those spectral lines of NO that do not fall within the SABER bandpass but that nevertheless are substantial emitters of energy. To illustrate this issue, we show in Figure 2 a computed limb radiance spectrum for NO at 135 km tangent altitude, along with the SABER relative spectral response function. As is evident in the figure, there is substantial emission outside of the SABER bandpass that needs to be accounted for in determining the total energy emitted by NO.

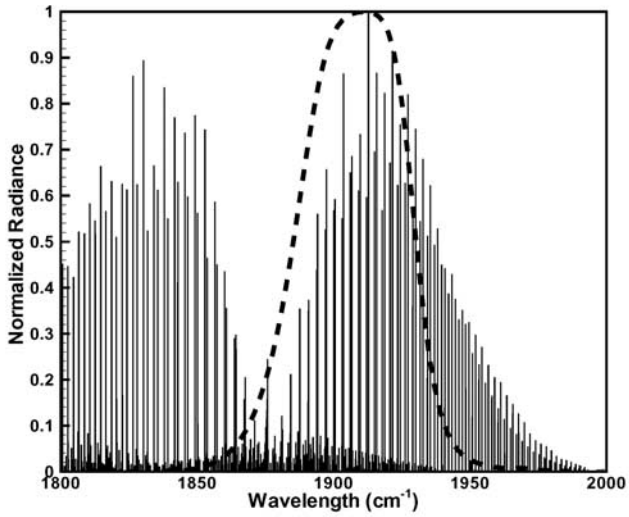

Figure 2. Normalized NO 5.3 μm limb radiance spectrum with the SABER relative spectral response function overlaid.

[18] The quantity E that we desire is a vector (equivalently a vertical profile as a function of altitude) whose elements E_j are given by equation (3) but with φ_i equal to 1.0 for all lines of NO, including those outside of the nominal bandpass of SABER. The elements E_j are then given by

$$\mathrm{E}_j = hc \sum_{i=1}^{k} V_{ij}\ \nu_i. \tag{4}$$

The units of the elements E_j are also energy per volume per time. In order to derive E_j from the rates e_j determined from inversion of the SABER limb radiance profile, we define and precalculate an "unfilter" factor U, a vector whose elements u_j are

$$\mathrm{u}_j = \frac{\mathrm{E}_j}{\mathrm{e}_j}. \tag{5}$$

The unfilter factor is the ratio of the total volumetric emission rate of energy (all lines, all bands) from NO at a given altitude (E_j) to the emission sensed by the SABER instrument as modified by the spectral response function of the instrument (e_j). It is straightforward to show from the radiative transfer equation that the elements u_j are formally given by

$$\mathrm{u}_j = \frac{\sum_{i=1}^{k} S_{ij}J_{ij}}{\sum_{i=1}^{k} S_{ij}J_{ij}\varphi_i}. \tag{6}$$

In equation (6), S_{ij} is the line strength (cm^{-1}/molecule cm^{-2}) and J_{ij} is the source function (erg cm^{-2} sr s cm^{-1}) of

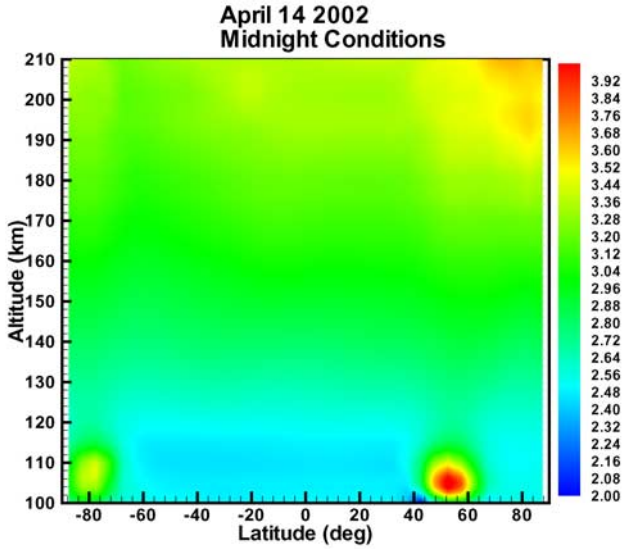

Figure 3a. Zonal mean "unfilter factors," the ratio of the total energy emitted by NO to that emitted within the SABER NO channel bandpass as a function of altitude, for midnight conditions on 14 April 2002.

the ith spectral line at conditions at altitude j. The source function is defined identically in equations (6) and (1). The summation is again over all lines and bands of the molecule.

[19] The unfilter factor of equation (6) may be computed explicitly by specification of the vibrational and rotational temperatures (T_v and T_r) for each line so that the line strength and source functions may be appropriately computed for the conditions of nonlocal thermodynamic equilibrium (non-LTE) that occur in the thermosphere for NO. The unfilter factor may also be computed by simulating the limb radiances for SABER under non-LTE conditions (with the T_v and T_r specified), with and without the SABER spectral response function, performing the inversions to determine the volume emission rates of energy E_j and e_j, and then computing the ratio u_j. We choose the latter approach of evaluating equation (5) since our computer codes readily evaluate these quantities, and we do so for both quiescent and storm conditions. Our value of E_j is then determined by taking the modeled u_j and multiplying it by the value of e_j obtained by inverting the SABER limb radiance.

[20] Shown in Figures 3a and 3b are zonal cross sections for quiescent conditions and storm conditions at night of the computed unfilter factor u_j between 100 and 210 km altitude. These values are obtained using the model of *Funke and Lopez-Puertas* [2000] to determine the vibrational and rotational temperatures of NO from which the limb radiance is simulated. The atmospheric inputs for this computation come from the ASPEN general circulation model for storm conditions. We show night only conditions since the SABER observations for the April 2002 storm period are almost entirely at night, although our calculations do indicate a small diurnal variation in the u_j values.

[21] Despite the greatly different geophysical conditions, the unfilter factors u_j are almost identical above 110 km in either storm or quiescent conditions, as seen in Figures 3a and 3b. Below 210 km, the standard deviation of the mean of the zonal mean unfilter values is only a few percent of the mean. Therefore we adopt and apply only one (i.e., the mean of the zonal mean) value of the unfilter factor at all latitudes. We consider altitudes below 210 km because the radiated energy from NO is almost entirely below this altitude, as can be inferred from the radiances shown in Figure 1. These unfilter values demonstrate that about 40% of the total NO radiance falls within the bandpass at 100 km, while only about 28% falls within the bandpass at 200 km.

[22] The unfilter factor is applied to each measured profile of NO volume emission rate recorded by the SABER instrument to obtain globally the total rate of emission from NO. Shown in Figures 4a and 4b are zonal mean contours of the volume emission rate of energy for day 104 (14 April 2002 prestorm, Figure 4a) and day 109 (19 April 2002 storm time, Figure 4b) conditions. Note the difference in scale between the two figures. The zonal mean emission rates are up to three times larger at the highest latitudes during the storm than before. These emission rates are comparable to those shown by *Mlynczak et al.* [2003] except that the present values are as much as 20% smaller at 200 km due to a smaller unfilter factor being used in the present calculation. The difference between the present and prior calculations is that rotational non-LTE is more accurately accounted for in the present unfilter factor determination. It can be shown that the unfilter factor depends strongly on the value of the rotational temperature as this governs the relative intensity of the individual lines and hence their weighting by the spectral filter. This behavior will be treated fully in subsequent publications describing the SABER scientific algorithms. The results of *Mlynczak et al.* [2003] remain unaltered by this reduction in u_j at the highest altitudes and are in fact within the stated error bounds of the original paper.

[23] To check the accuracy of the unfilter factor calculations, we have compared values computed above with

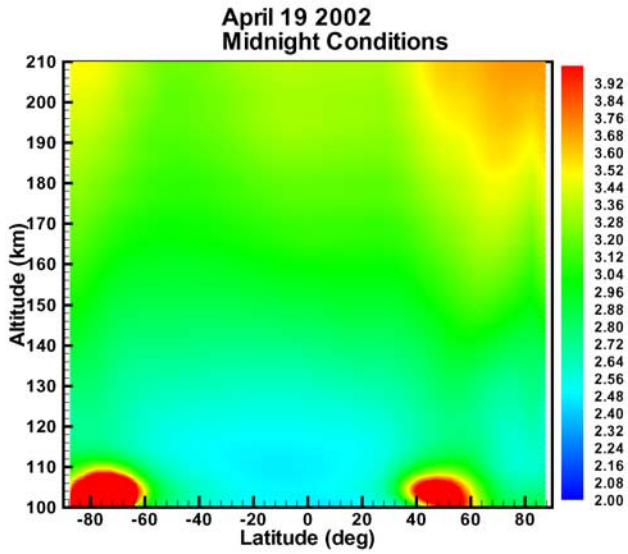

Figure 3b. Zonal mean "unfilter factors," the ratio of the total energy emitted by NO to that emitted within the SABER NO channel bandpass as a function of altitude, for midnight conditions on 19 April 2002.

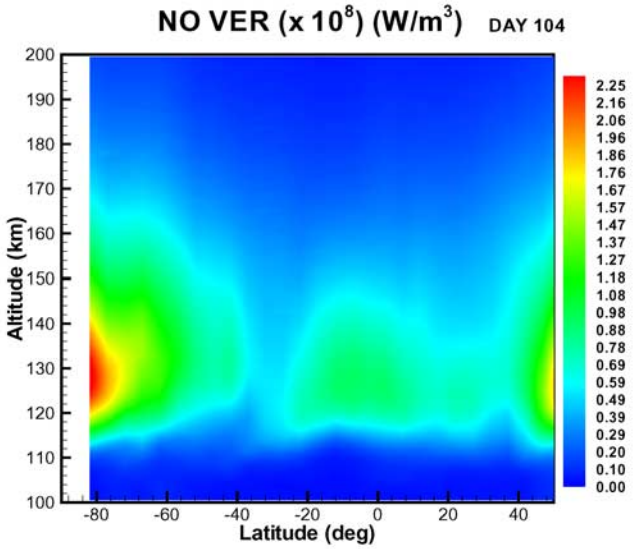

Figure 4a. Zonal mean energy loss rates (W/m^3) for NO as determined from SABER limb radiance measurements, for 14 April 2002 quiescent conditions.

those derived from direct integration of measured NO emission spectra. The MIPAS instrument on the Envisat satellite measures NO emission spectra. The unfilter factor can be computed by inverting the spectra and integrating with respect to wave number, with and without including the SABER relative spectral response. Preliminary comparisons show the MIPAS-derived factor to be within 3% of the factors computed above at 122 km and at 163 km altitude (J. Gardner, Air Force Research Laboratory, private communication, 2005).

3.1.1. Energy Loss Rates in Kelvin Per Day

[24] In order to illustrate the magnitude of the energy loss it is instructive to convert the rates from units of energy per time per volume to rates in Kelvin per day. We do so through the first law of thermodynamics at each altitude by

$$E_j = \rho\, C_p \frac{\partial T}{\partial t}. \tag{7}$$

In equation (7) ρ is the density and C_p is the heat capacity at constant pressure. The atmospheric density is taken from the ASPEN model and the heat capacity is computed appropriately based on the abundance of N_2, O_2, and O from the ASPEN model.

[25] In this analysis we solve for $\partial T/\partial t$ but emphasize that this is an upper bound on the radiative cooling rate due to emission from NO. Cooling occurs when energy is drawn into the NO molecule through collisions and subsequently radiated. The analysis of the SABER data yields an energy loss rate indicative of all processes causing NO to radiate. In particular, the energy radiated by NO subsequent to excitation by exothermic reactions reduces the heating due to those reactions, but since it has never entered the thermal field, it cannot cool the atmosphere. Rather, the chemiluminescent emission subsequent to the reactions simply reduces the heating efficiency of the reactions to some value less than unity. Under quiescent conditions the chemiluminescent emission is as much as 4–5% of the total NO emission [*Funke and Lopez-Puertas*, 2000]. This fraction is expected to increase during storm times, depending on the relative effects of N-atom increases versus increases in atomic oxygen at a given altitude. However, even under storm conditions, the dominant NO emission term will still be from collisions with atomic oxygen and not from chemiluminescence. Nevertheless, the chemiluminescent energy originates in the energy deposited into the atmosphere from the solar storm and contributes to the overall thermostat effect. The energy loss rate expressed in K/day is simply another way to express the quantity of energy radiated by NO during the storm. The true NO cooling rate is less than or equal to the values derived here.

[26] Shown in Figures 5a–5d are the rates of energy loss in Kelvin per day (K/d) derived from the SABER energy loss rates E_j, for conditions prior to and during the storm. The values shown in Figures 5a–5d are zonally averaged energy loss rates for the specified days. Shown are figures for day 104 (prestorm, Figure 5a) and day 109 (storm time, Figure 5b). Instantaneous energy loss rates determined during the storm time are found to exceed 2000 Kelvin per day near 50°N latitude. The difference between the energy loss rates from day 109 and 104 is shown in Figure 5c. Note the change in scale between the figures. Figure 5c illustrates the essence of the thermostat effect, whereby the enhanced radiative emission by NO during the storm period increases the energy loss by as much as 1600 Kelvin per day at the peak energy loss rate and by over 1000 Kelvin per day over a wide range of latitudes and altitudes. In Figure 5d we show a single profile of the maximum radiative loss rate at 52°N. The rate of energy loss derived from SABER coupled with the atmospheric density from ASPEN combine to yield an effective energy loss rate maximizing in excess of 2200 Kelvin per day near 180 km on 19 April. The energy loss rate (which likely is the radiative cooling rate under quiescent

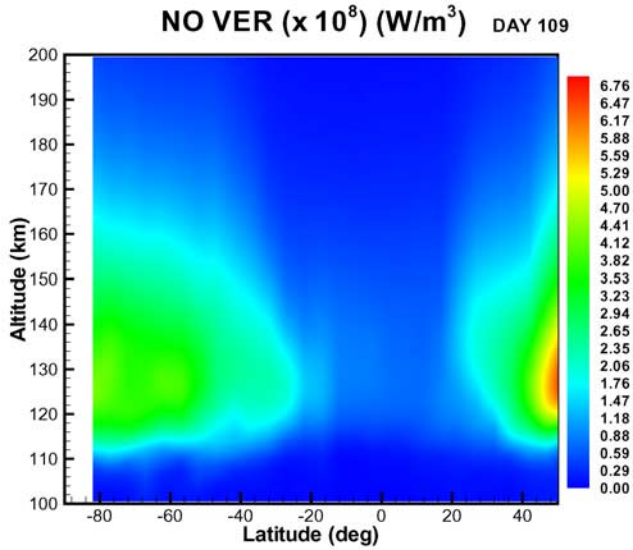

Figure 4b. Zonal mean energy loss rates (W/m^3) for NO as determined from SABER limb radiance measurements, for 19 April 2002 storm conditions. Note the change in scale from Figure 4a.

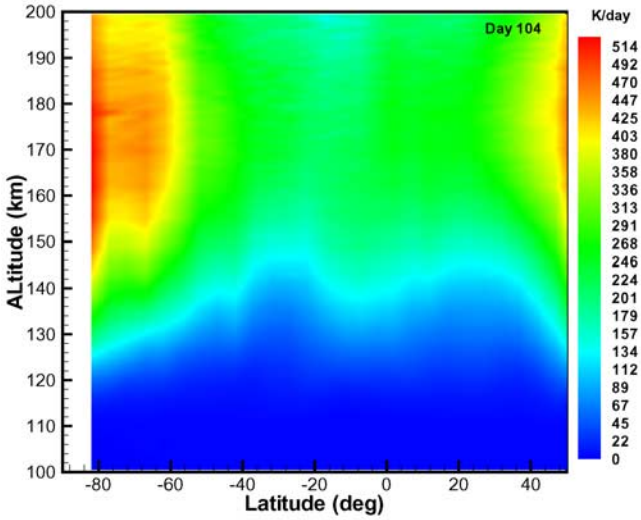

Figure 5a. Energy loss rates in K/day for 14 April 2002 (quiescent conditions) derived from SABER energy loss rates shown in Figure 4a.

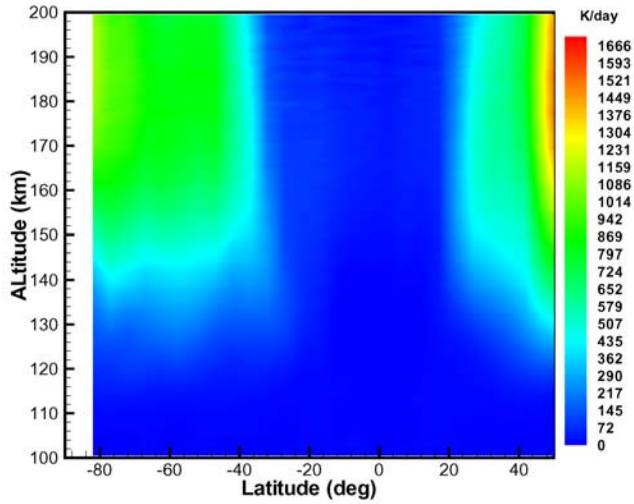

Figure 5c. The difference in energy loss rates, in K/day, between 19 April 2002 and 14 April 2002. This is the essence of the thermostat effect of NO.

conditions) is about 500 K/day several days before the storm on 14 April.

3.2. Computation of Fluxes of Radiant Energy

[27] The next step toward computing the total amount of energy radiated by NO during the storm period is to compute the fluxes of radiant energy (energy per area per time) emitted by NO in the thermosphere. The flux F (ergs cm^{-2} s^{-1}) is obtained from each vertical profile of volume emission rate of energy E_j by integrating with respect to altitude, i.e.,

$$F = \int_{z_1}^{z_2} E(z)dz. \tag{8}$$

For our purposes the limits of integration are 100 km to 210 km. The flux F is the total amount of radiant energy exiting the thermosphere due to emission from NO. Because the profile of emission rate E_j accounts for radiation emitted in all directions, half of the flux exits the bottom of the thermosphere and half exits the top. The quantity F is the sum of the upwelling and downwelling streams of radiation.

[28] One of the key assumptions in the computation of the flux is that all of the energy emitted by NO escapes the thermosphere. In section 3.1 we showed that the absorption along the limb view (with approximately a 2000 km pathway through the atmosphere and an approximate 300 km path length through the tangent layer) was minimal. From this we can directly infer that all radiation emitted by NO exits the thermosphere as the path lengths over all solid angles are shorter than in the limb view. To verify this with a different approach, we have computed

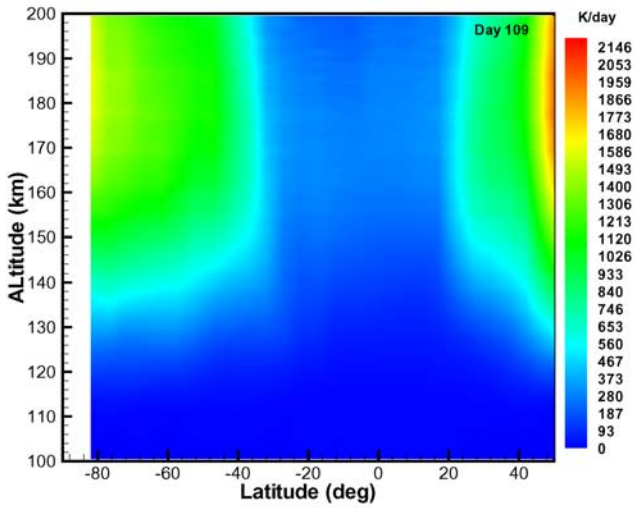

Figure 5b. Energy loss rates in K/day for 19 April 2002 (storm conditions) derived from SABER energy loss rates shown in Figure 4b. Note change in scale from Figure 5a.

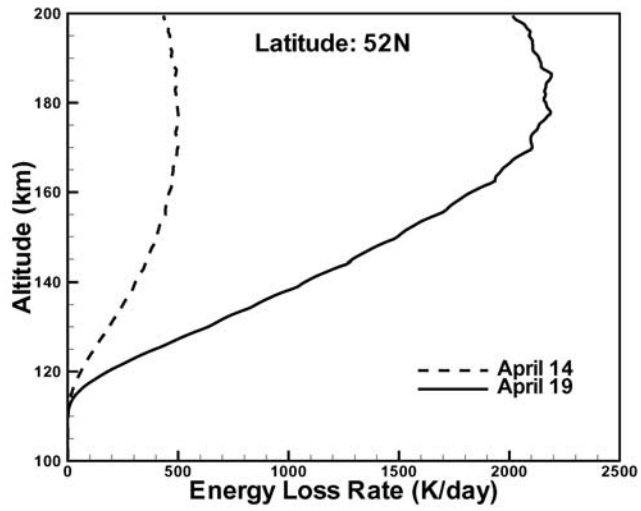

Figure 5d. Example of individual energy loss rate profiles derived on 14 April and 19 April at 52 N latitude. The peak energy loss rate exceeds 2200 K/day at this latitude on 19 April.

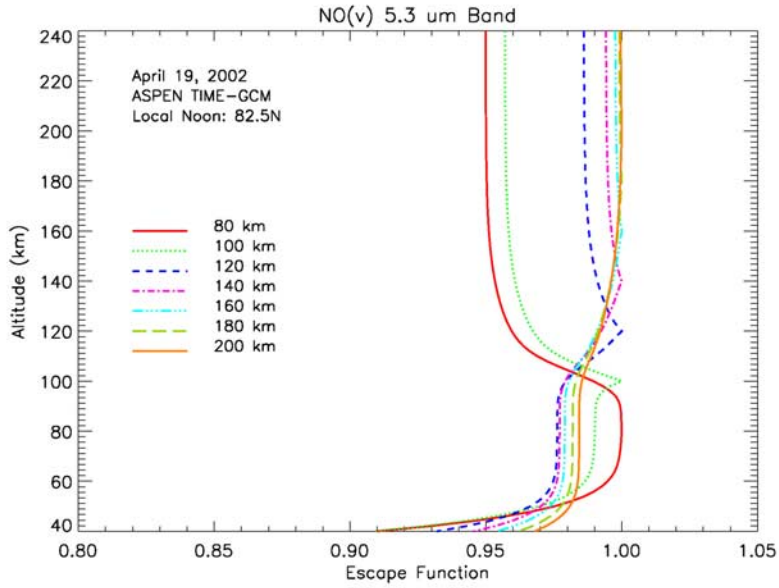

Figure 6. Escape functions $\Gamma(z, z')$ for NO under storm conditions at altitudes of 80, 100, 120, 140, 160, 180, and 200 km. These functions indicate that photons emitted by NO at these altitudes have a high probability (>95%) of escaping the thermosphere.

the escape function for radiation, $\Gamma(z, z')$, which describes the probability of a photon emitted at altitude z arriving at altitude z' before being absorbed. The escape function is given by the expression:

$$\Gamma(z,z') = \frac{1}{S(z)} \int k_\nu(z) E_2[\Delta\tau_\nu(z,z')] d\nu \tag{9}$$

In equation (9), $S(z)$ is the absorption band strength at altitude z, E_2 is the second exponential integral, and $\Delta\tau_\nu(z, z')$ is the vertical optical mass between altitude z and z'. Shown in Figure 6 are the escape functions for altitudes z of 80, 100, 120, 140, 160, 180, and 200 km. It is clear from this figure that photons emitted at 80 km or above escape the thermosphere. Those emitted upward escape to space while those emitted downward are absorbed in the lower mesosphere or below. Figure 6 confirms the assumption that virtually all of the radiation emitted by NO exits the thermosphere.

[29] The fluxes of radiation were also computed and presented by *Mlynczak et al.* [2003] in their Figures 4a–4b and 5a–5d. These show the global extent and time evolution of the elevated NO emission. These prior results indicated that the storm persisted for approximately 3–4 days, at least as inferred by the enhanced levels of NO emission. We have recomputed the fluxes here based on the new unfilter factors u_j and have found only minor changes in the fluxes from those given by *Mlynczak et al.* [2003].

[30] Shown in Figure 7 are the zonal mean fluxes for days 104–113, over the range of latitudes observed by SABER. Clearly indicated is the increase in the radiated flux for days 107–111, especially at high latitudes. The maximum instantaneous fluxes are on the order of 2.5×10^{-3} W/m^2 (2.5 mW/m^2). Note by comparison the average top-of-atmosphere infrared flux the entire planet is approximately 250 W/m^2, $\sim 10^5$ times larger. This comparison of the scales of energy strongly suggests that while the solar storms dramatically altered the thermosphere, they did not contain substantial energy to directly alter the planetary climate or energy balance. Any such effects would have to come through indirect mechanisms, i.e., alteration of planetary circulation or through modifications of the key chemical species such as ozone, as was observed in the October/November 2003 storms [*Seppälä et al.*, 2004].

3.3. Computation of Radiated Power

[31] The instantaneous power is the energy per unit time radiated by the NO molecule. The power P is obtained by integrating the fluxes F (as derived in the prior section) with respect to area,

$$P = \int F \, dA. \tag{10}$$

We evaluate the power P in bins of 5 degrees of latitude. If we assume the SABER fluxes F to be uniformly distributed in longitude, the total power $P(\lambda)$ radiated in each 5 degree bin of latitude (λ) is given by

$$P(\lambda) = \bar{F}(\lambda) A(\lambda), \tag{11}$$

where $F(\lambda)$ is the zonal mean flux in each 5 degree bin and $A(\lambda)$ is the area of the 5 degree strip of latitude taken around 360 degrees of longitude. $A(\lambda)$ is computed by the expression

$$A(\lambda) = 2\pi R_e^2 (\sin(\lambda_2) - \sin(\lambda_1)), \tag{12}$$

where R_E is the Earth's radius and λ_2 and λ_1 are the limits of the latitude bins and $\lambda_2 - \lambda_1 = 5$ degrees.

[32] Shown in Figure 8 are plots of the zonal mean instantaneous radiated power as a function of latitude for

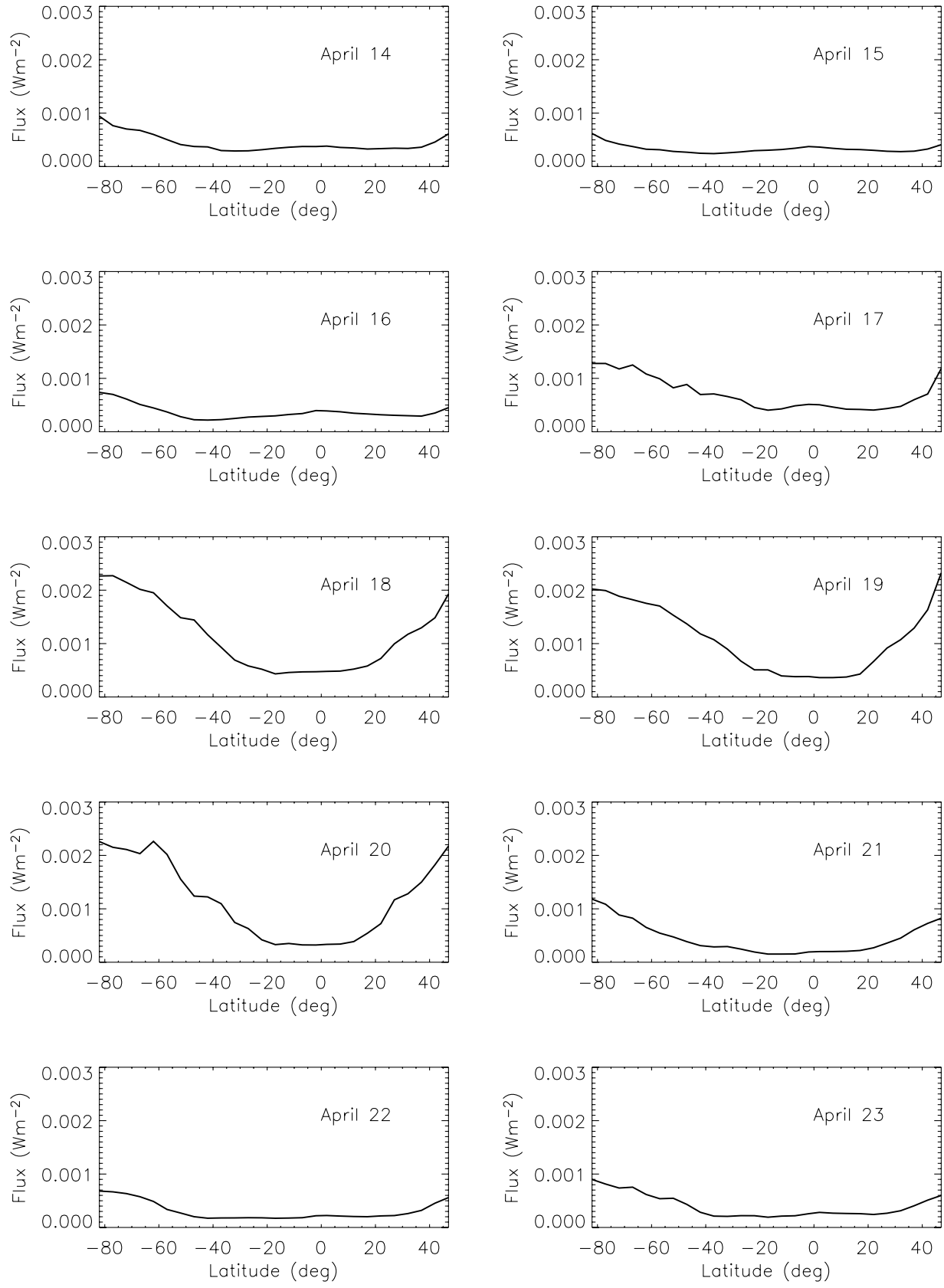

Figure 7. Zonal mean fluxes (W/m^2) of energy emitted by NO in the thermosphere for days 104 (14 April 2002) through day 113 (23 April 2002). Note the large increases at middle and high latitudes on days 107 through 111 (17 April through 21 April) of 2002.

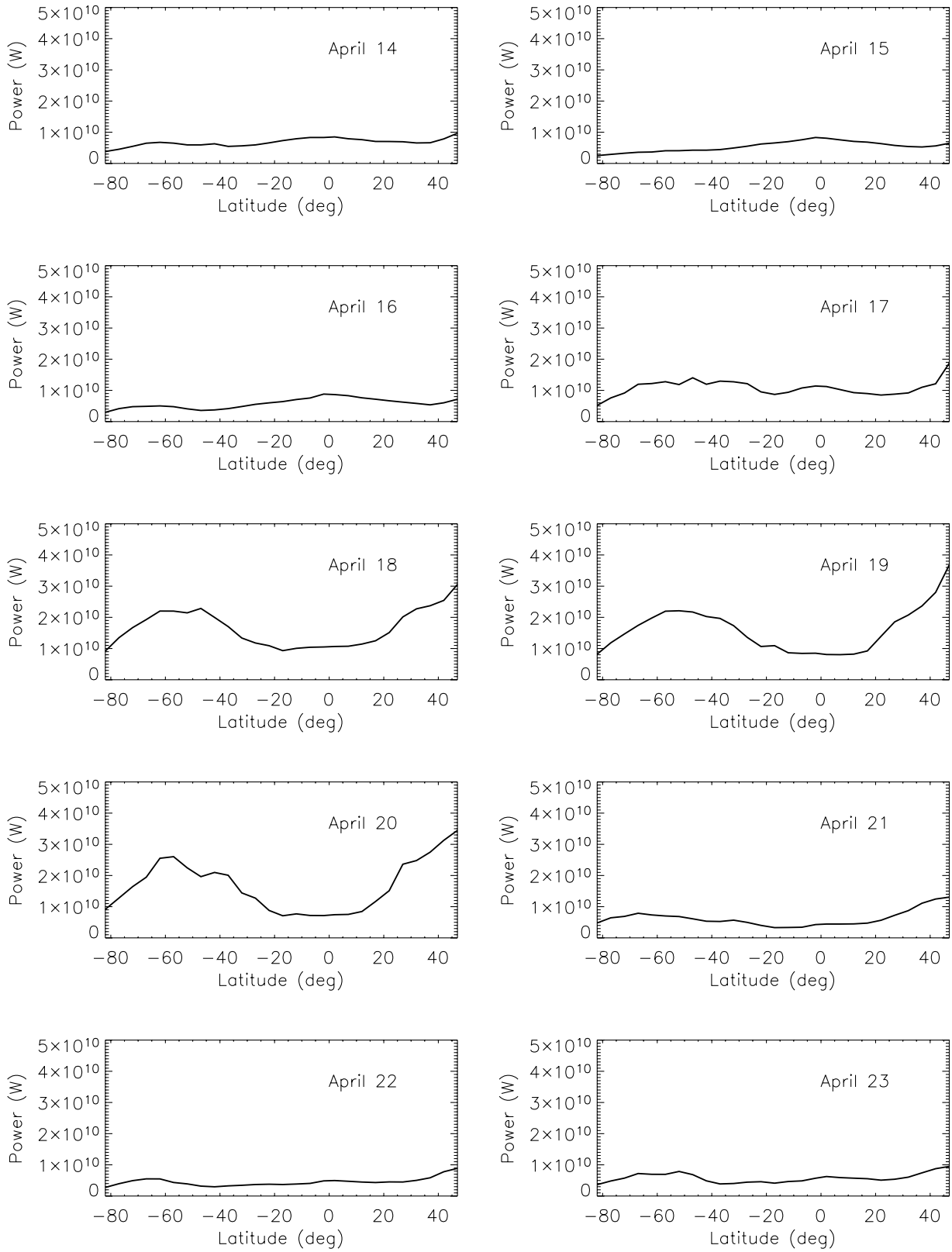

Figure 8. The zonal mean power (Watts) emitted by NO in the thermosphere for days 104 through 113 of 2002. In contrast to the fluxes in Figure 10 the power peaks at subpolar latitudes and decreases toward the pole. Maximum observed emitted power is about 4.5°E + 10°W.

days 104 through 113. Note that in contrast to the radiated fluxes, the radiated power peaks at latitudes around 50 degrees in the southern hemisphere. The lack of SABER coverage above 50 degrees north at this time precludes determination of the latitude at which the radiated power peaks in the northern hemisphere. However, we note that by definition the radiated power must go to zero at the poles. The peak radiated power in the northern hemisphere derived here is in excess of 4×10^{10} W on 19 April. The power in Figure 8 shows a rather uniform distribution as a function of latitude prior to and after the storm, with peak power occurring at high latitudes but away from the poles during the storm. There is a clear hemispheric asymmetry in the radiated power during the storm. The elevated power amounts over the background levels clearly indicate the effects of the storm are present on 17–20 April, with perhaps the suggestion of some high northern latitude effects on 21 April.

3.4. Computation of Radiated Energy Through Temporal and Meridional Integration

[33] We have now progressed to the point where we have the instantaneous radiated power as a function of latitude for days prior to, during, and after the storm events of April 2002. The latitude coverage extends from the South Pole to 53 degrees north latitude, as limited by the position of the SABER instrument on the TIMED spacecraft. In order to derive the total energy radiated by NO we must integrate the power with respect to time. This presents a fundamental challenge because the SABER observations are essentially at fixed local times and it is likely that the NO emission varies over the course of the day. The SABER observations are essentially all during twilight or night during the April 2002 storm period. Shown in Figure 9 is a plot of the local time of SABER observations as a function of latitude for day 104 and day 109 showing the SABER observations near 0500 and 1900 local time except near the north and south limits of orbital coverage. SABER is able to observe two local times daily (ascending and descending node) by virtue of continuously observing infrared emission.

[34] In order to examine the possible temporal variation of the NO emission, we have used the ASPEN simulations to compute the total power radiated by NO in hourly time steps at each latitude, before the storm on day 104 and during the storm on day 109. Shown in Figure 10 are the results of these simulations for two latitudes, 57°S and 22°S. As is evident, on day 104, prior to the storm, at low latitudes, there is a marked diurnal variation of the NO power. On day 109, during the storm, the effects of the storm are predicted to be so intense that the natural diurnal signal is overwhelmed. At high latitudes the modest diurnal variation is also completely changed during storm conditions.

[35] We have examined and rejected an approach to temporally integrate the SABER data that would normalize SABER temporally to the ASPEN model. The only plausible assumption, given the paucity of SABER local time sampling, is that the SABER power relative to the ASPEN power is constant at all local times. It can be shown mathematically that this assumption leads simply to equating SABER and ASPEN power and radiated energy, thus providing no true temporal integration.

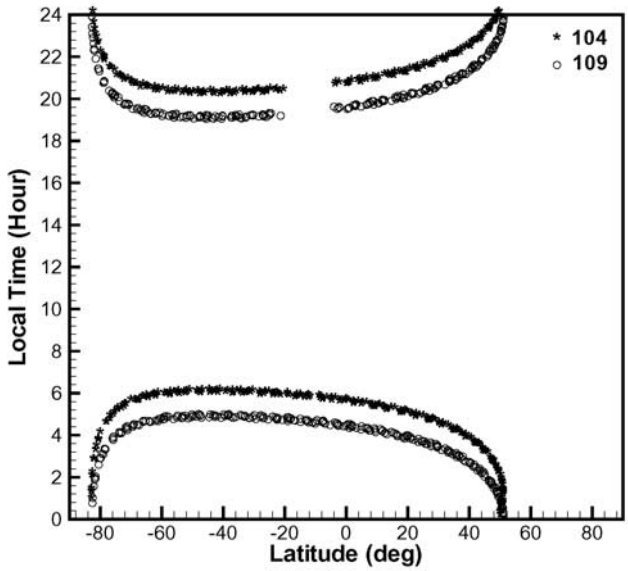

Figure 9. SABER local time sampling as a function of latitude on 14 April 2002 (day 104) and 19 April 2002 (day 109) illustrating the limited temporal sampling.

[36] We therefore estimate the energy emitted by taking the zonal average power (e.g., Figure 8) for all local times measured by SABER and multiplying it by the length of day (86400 s) to obtain an estimate for each day of the energy E_S radiated in each 5 degree latitude band. We then integrate E_S meridionally in order to compute the total globally radiated energy E_T according to the relation

$$E_T = \int E_s(\lambda)\cos(\lambda)d\lambda. \tag{13}$$

[37] Listed in Table 2 are the results of these estimates of the daily global radiated power and energy from nitric oxide from day 104 of 2002 (14 April) through day 113 (23 April). There are six entries in the table for each day. The first column is the radiated power for the southern hemisphere between the equator and 52°S latitude; the second column is the power between 52°S and the South Pole; the third column is the radiated power between the equator and 52°N. These three columns are derived from the SABER observations. The fourth column is the estimated global radiated power between 52°N and the North Pole estimated from the ratio of the northern hemisphere and southern hemisphere data in the first three columns. The fifth column is the sum of the first four columns. The sixth column is the energy in ergs obtained by multiplying the power in column 5 by the length of day or 86,400 s.

[38] To estimate the energy emitted as a consequence of the storm, we assume that the conditions on days 104 to 106 and 111 to 113 are quiescent or background days. The average radiated energy for these 6 days is 1.22×10^{23} erg. The total radiated energy for days 107 through 110 is approximately 12.5×10^{23} erg. Subtracting the background 1.22×10^{23} erg for each of the 4 days leaves a total estimated radiated energy from NO for the April 2002 storm period of about 7.7×10^{23} erg, or equivalently 2.1×10^{36} photons of 5.3 μm wavelength.

[39] The estimated amount of energy input into the upper atmosphere through Joule heating and auroral dissipation is about 2.7×10^{24} ergs over the storm period. This estimate is based on the Assimilative Mapping of Ionospheric Electrodynamics (AMIE) procedure [*Richmond and Kamide*, 1988] by combining various direct and indirect measurements from space- and ground-based instruments. See *Lu et al.* [1998] for more information. Our estimate of NO emission accounts for approximately 28% of the storm energy.

4. Emission From Carbon Dioxide

[40] The other energetically significant emission observed by SABER during the storm period is from carbon dioxide (CO_2) at 15 μm. SABER observes emission from CO_2 at 15 μm in two different spectral channels, a "wide" channel in which emission from all of the CO_2 bands at 15 μm would be detected, and a "narrow" channel that concentrates on emission from the q-branch of the 15 μm fundamental band. The two spectral intervals are used by SABER in order to derive temperature according to the "two color" approach [*Gille and House*, 1971] for infrared limb sounding. To analyze the CO_2 emission, we choose the data from SABER channel 3, the second of two "wide" channels. As indicated in Table 1, the bandpass for this channel is 579 to 763 cm^{-1} or 17.3 to 13.1 μm. The channel is sufficiently broad and the relative spectral response is nearly equal to 1.0 over the bandpass that to first order that the "unfilter factor" for this channel can be taken as 1.0. We then follow the approach as outlined above for NO: weak line inversion to obtain volume emission rates of energy, vertical integration to obtain fluxes of energy, zonal averaging and integration with respect to area, meridional integration, and temporal integration. We again assume that the emission in the limb view is in the weak line limit and therefore follow the same approach as for NO to determine volume emission rates. Our experience with the SABER data and the carbon dioxide amounts in the lower thermosphere strongly suggest that the assumption of the weak line radiative transfer regime is valid above 105 km.

[41] Shown in Table 3 for days 104 through 113 is the estimate of the radiated energy from carbon dioxide. Similar to the results for NO, we display values for the northern hemisphere and southern hemisphere observed by SABER and estimated values for the part of the northern hemisphere not observed by SABER. The total global power is given as is the estimate of radiated energy for each day. Clearly, the response of CO_2 is much smaller than that of NO. We estimate the additional energy radiated by CO_2 during the 4 storm days to be 1.8×10^{22} ergs. This is approximately 2.3% of the energy radiated by NO. We therefore conclude that although CO_2 exhibits a radiance enhancement, its effects in removing storm energy are quite small relative to NO and therefore contributes only a minor amount to the overall thermostat effect.

5. Emission From the Atomic Oxygen Fine Structure Line at 63 μm

[42] *Bates* [1951] suggested that emission from the fine structure line of atomic oxygen was an important radiator in the thermosphere. The 63-μm emission line of atomic oxygen is difficult to observe because of its relatively weak signal and the technical challenges associated with observing far-infrared emission from space-based platforms. The 63-μm emission has been observed in a handful of rocket experiments [*Grossman and Vollmann*, 1997], from balloon-borne instruments [*Mlynczak et al.*, 2004], and most extensively from the CRISTA instrument payload that flew on the space shuttle [*Grossman et al.*, 2000]. There are no known observations of this emission during the solar storm event of April 2002. We rely on simulations of the storm event by the ASPEN model from which we compute the rates of infrared cooling to assess whether or not a thermostat effect is expected with atomic oxygen in response to the solar storm event.

[43] To assess the existence of a thermostat effect in atomic oxygen, we use ASPEN model values of kinetic temperature and atomic oxygen abundance and compute the vertical profile of radiative cooling at 63 μm between 100 and 210 km. The cooling rate is computed under the assumption of local thermodynamic equilibrium (LTE) which is thought to hold for this transition below 300 km [*Sharma et al.*, 1994]. The radiative cooling rate, expressed in terms of K/d, is derived from the expression

$$\frac{\partial T}{\partial t} = \frac{g}{C_p}\frac{\partial F_{net}}{\partial p}. \tag{14}$$

In equation (14), g is the acceleration due to gravity, C_p is the heat capacity at constant pressure, and $\partial F_{net}/\partial p$ is the divergence of the net radiative flux. The fine structure line is not in the weak line limit of radiative transfer over much of the range in which it is important to cooling the lower thermosphere. We therefore compute the radiative cooling rate using the line-by-line radiative transfer code described by *Kratz et al.* [1998, 2005] with no limiting assumptions on radiative transfer regimes. Upwelling and downwelling fluxes and their divergences are computed based on the ASPEN model profiles of temperature and atomic oxygen. The heat capacity is computed appropriately for the abundance of diatomic and monatomic species, and the cooling rate is determined.

[44] Shown in Figures 11a and 11b are the zonal mean radiative cooling rates for midnight conditions on day 104 (prior to the storm onset) and on day 109 (during the storm). The calculated cooling rate is not large to begin with, maximizing around 60 K/day at 200 km. This value is only about 10% of the NO cooling at high latitudes under quiescent conditions. In Figure 11c is the difference in cooling rate between days 109 and 104. As can be seen, there is not a marked difference in the cooling rate between the 2 days, in strong contrast to the change in the NO and CO_2 emissions. The change in cooling by atomic oxygen is less than 10 K/day over most altitudes and latitudes (except approaching 20 K/day near the poles), implying a much smaller change in energy loss rates than in NO or CO_2, at least in an absolute sense. We therefore conclude that there is no substantial "thermostat" effect in atomic oxygen emission at 63 μm.

[45] The effective absence of a thermostat effect in atomic oxygen emission is explained as follows. First, the source function for this atomic oxygen emission is identical to the Planck blackbody function under the assumed conditions of

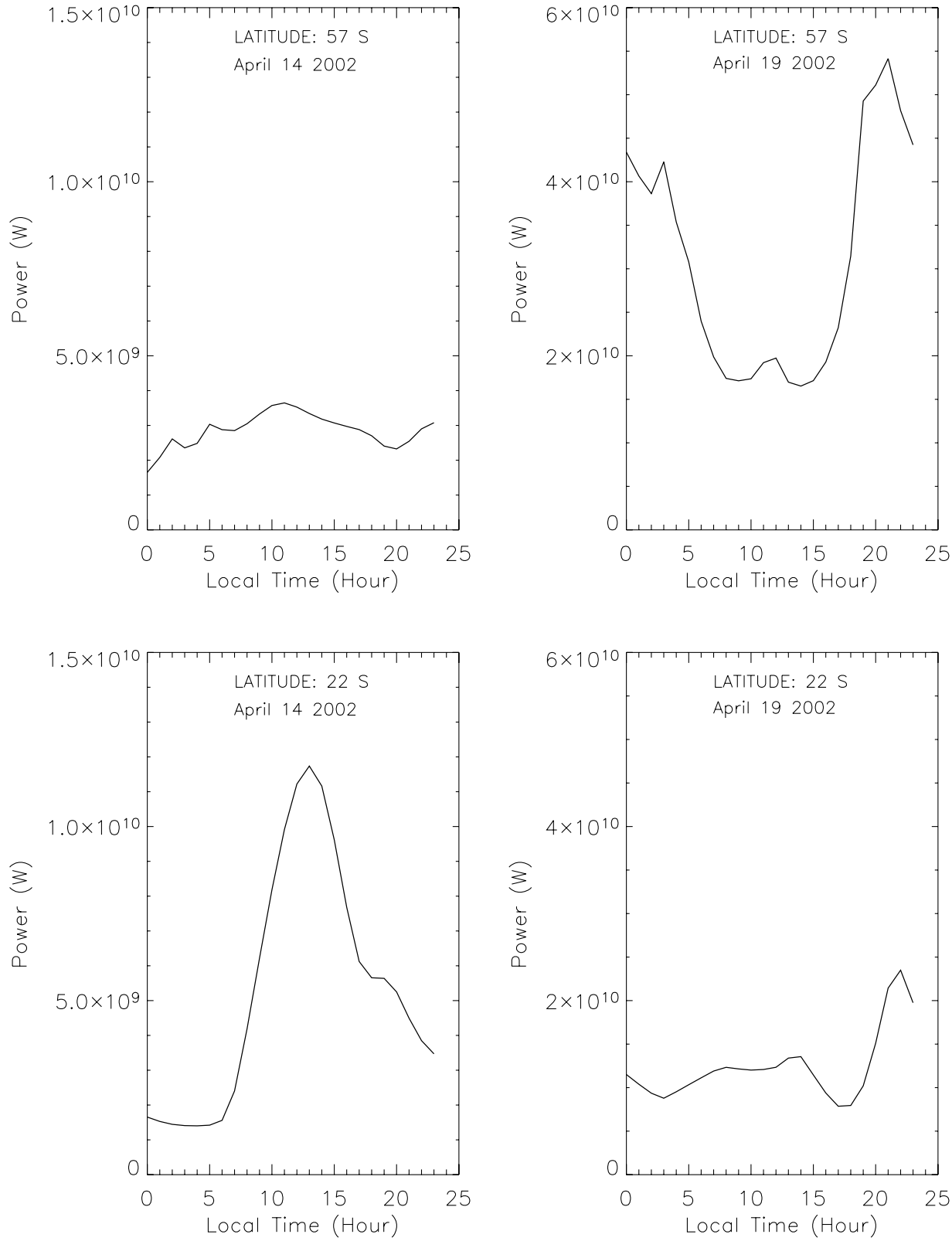

Figure 10. Local time variation of power (W) emitted by NO as estimated from the ASPEN model for 14 April 2002 (left-hand column) and 19 April 2002 (right-hand column) for latitudes of 57°S and 22°S. The natural diurnal variation is completely changed during the storm period.

Table 2. NO Average Power (watts) in Four Separate Latitude Bands, Global Average Power (watts), and Total Energy (ergs) Radiated By NO for Days 104 Through 113 of 2002

Day	SH 0–52	SH 52–90	NH 0–52	NH 52–90[a]	Total *P*	Energy, erg
104	0.642E+11	0.125E+11	0.740E+11	0.144E+11	0.165E+12	0.143E+24
105	0.559E+11	0.734E+10	0.619E+11	0.812E+10	0.133E+12	0.115E+24
106	0.550E+11	0.970E+10	0.667E+11	0.117E+11	0.143E+12	0.124E+24
107	0.106E+11	0.226E+11	0.109E+12	0.232E+11	0.261E+12	0.225E+24
108	0.129E+12	0.393E+11	0.176E+12	0.537E+11	0.398E+12	0.343E+24
109	0.132E+12	0.364E+11	0.170E+12	0.470E+11	0.385E+12	0.333E+24
110	0.119E+12	0.430E+11	0.180E+12	0.651E+11	0.408E+12	0.352E+24
111	0.435E+11	0.146E+11	0.708E+11	0.238E+11	0.153E+12	0.132E+24
112	0.353E+11	0.990E+10	0.523E+11	0.147E+11	0.112E+12	0.969E+23
113	0.469E+11	0.132E+11	0.618E+11	0.175E+11	0.139E+12	0.120E+24

[a]Estimated for NH 52–90, from ratios of NH, SH data.

local thermodynamic equilibrium in the fine structure line. The Planck function at 63 μm is becoming linearly proportional to temperature, requiring substantial changes in temperature to achieve substantial changes in the source function and hence the emission. By comparison, NO emission is approximately 12 times more sensitive to changes in temperature than is the emission by atomic oxygen. Second, the ASPEN model predicts only modest changes in atomic oxygen in response to the storm. Hence the amount of emitter is not changing substantially. If the source function and the emitting species do not change significantly, the associated emission and cooling will not change substantially, either. On the basis of these physical principles we would not expect substantial changes in the O-atom 63-μm emission during the storm. The required changes in temperature or O-atom amounts are in fact so large as to be nonphysical.

6. Energy Loss Due to Heat Conduction

[46] Temperature gradients in the thermosphere are sufficiently large that molecular heat conduction becomes a significant mechanism by which energy is transported downward from the warmer to the cooler regions. During the solar storm time, the thermosphere heats up greatly, with the rate of temperature change due to the storm increasing with altitude. Thus the lapse rate of the atmosphere likely increases, thereby offering the potential for increased levels of heat conduction in response to the storm. Using the ASPEN model, we assess the magnitude of the changes in energy transport from the thermosphere due to heat conduction. Shown in Figure 12 is the vertically integrated energy loss rate (erg/s) from the thermosphere due to heat conduction for 15 April to 23 April derived from these simulations. We note the calculation considers only molecular heat conduction and not eddy heat conduction. The latter process does represent a cooling term between 160 and 110 km but is a small contribution to the total cooling.

[47] Following an approach similar to that for the radiative losses, we estimate the mean energy loss due to heat conduction over this time period to be $\sim 2.35 \times 10^{18}$ erg/s. The variation in the energy loss rate is about 5% peak to peak. There is a suggestion of an increase in thermospheric energy loss from conduction for 17–20 April, but this is only about a 4% increase. If we assume that the suggested increase during the storm period is due to increased conduction as a result of changes in the vertical temperature gradient, we compute an increase in energy conducted from the thermosphere of 3×10^{22} erg. This is approximately 3.8% of the energy radiated by NO and about 1.7 times the energy estimated to be radiated by CO_2. Thus conduction, while continuously occurring during the storm, does not significantly change but perhaps facilitates the loss of a small amount of energy relative to NO infrared emission during the storm.

[48] In summary, we estimate energy losses of approximately 7.7×10^{23} erg due to NO emission, 1.8×10^{22} erg due to CO_2 emission, negligible emission from atomic oxygen, and 3×10^{22} erg due to heat conduction. These losses sum to a total of 8.18×10^{23} erg, approximately 30% of the energy estimated to have entered the upper atmosphere. We point out, however, that not all of the storm energy is dissipated in the thermosphere, as

Table 3. CO_2 Average Power (watts) in the Northern Hemisphere and Southern Hemisphere, Global Average Power (watts), and Total Energy (ergs) Radiated by CO_2 for Days 104 Through 113 of 2002

Day	NH 0–52	NH 52–90[a]	SH 0–52	SH 52–90	Total *P*	Energy, erg
104	0.200E+11	0.255E+10	0.172E+11	0.219E+10	0.419E+11	0.362E+23
105	0.189E+11	0.222E+10	0.171E+11	0.200E+10	0.402E+11	0.348E+23
106	0.187E+11	0.229E+10	0.169E+11	0.208E+10	0.400E+11	0.345E+23
107	0.199E+11	0.253E+10	0.178E+11	0.226E+10	0.426E+11	0.368E+23
108	0.219E+11	0.291E+10	0.203E+11	0.270E+10	0.478E+11	0.413E+23
109	0.217E+11	0.304E+10	0.198E+11	0.277E+10	0.473E+11	0.409E+23
110	0.227E+11	0.308E+10	0.203E+11	0.275E+10	0.488E+11	0.421E+23
111	0.202E+11	0.266E+10	0.170E+11	0.225E+10	0.421E+11	0.364E+23
112	0.196E+11	0.250E+10	0.168E+11	0.215E+10	0.410E+11	0.354E+23
113	0.191E+11	0.224E+10	0.175E+11	0.205E+10	0.409E+11	0.354E+23

[a]Estimated for NH 52–90, from ratios of NH, SH data.

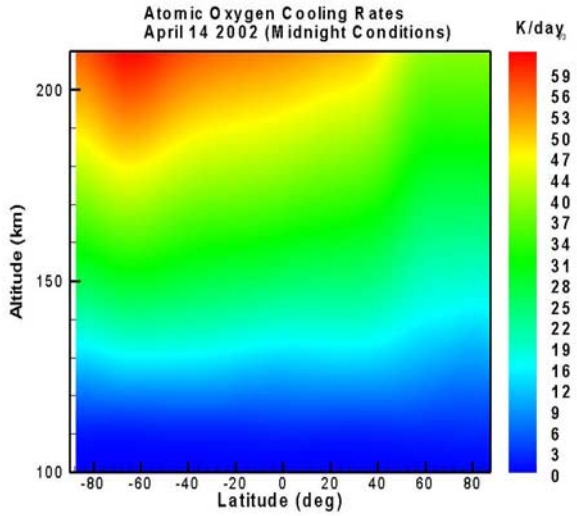

Figure 11a. The radiative cooling rate (K/day) at midnight due to emission from atomic oxygen at 63 μm on 14 April 2002 prior to the storm.

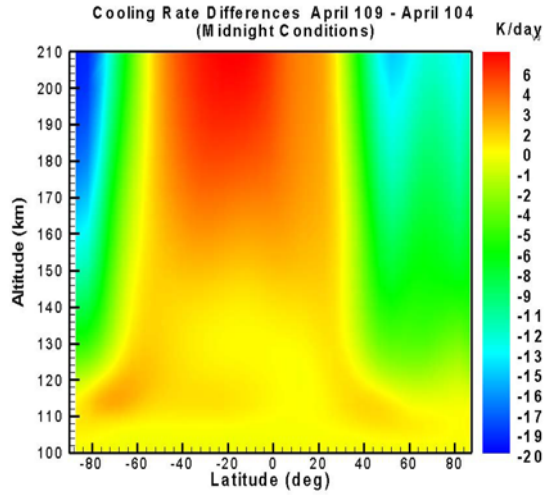

Figure 11c. The difference in the radiative cooling rates of Figures 14a and 14b, illustrating very little change in cooling by atomic oxygen due to the storm.

evidenced by the observed destruction of mesospheric ozone [*Seppälä et al.*, 2004].

7. Preliminary Assessment of Mechanisms Responsible for NO Radiance Enhancement

[49] Now that the relative importance of the three major infrared radiators and heat conduction in the thermosphere has been established, a key issue is to identify the mechanisms by which the NO radiation enhancement occurs. As indicated by *Mlynczak et al.* [2003], there are four mechanisms that could lead to an increase in NO emission. They are (1) increased NO abundance, (2) increased kinetic temperature, (3) increased atomic oxygen, and (4) increased rates of reaction leading to more chemiluminescent emission.

[50] To evaluate the relative importance of these mechanisms, we begin by looking in the lower thermosphere (below 140 km) at the NO concentrations recorded by the HALOE instrument on the Upper Atmosphere Research Satellite. Shown in Figures 13a and 13b are the ratios of the daily zonal mean NO concentrations measured by HALOE on 20 and 21 April (during the storm) to the daily zonal mean NO concentrations measured on 9 and 10 April

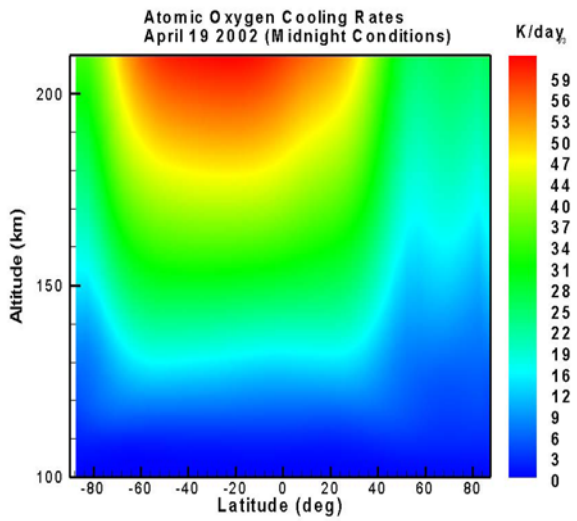

Figure 11b. The radiative cooling rate (K/day) at midnight due to emission from atomic oxygen at 63 μm on 19 April 2002 during the storm.

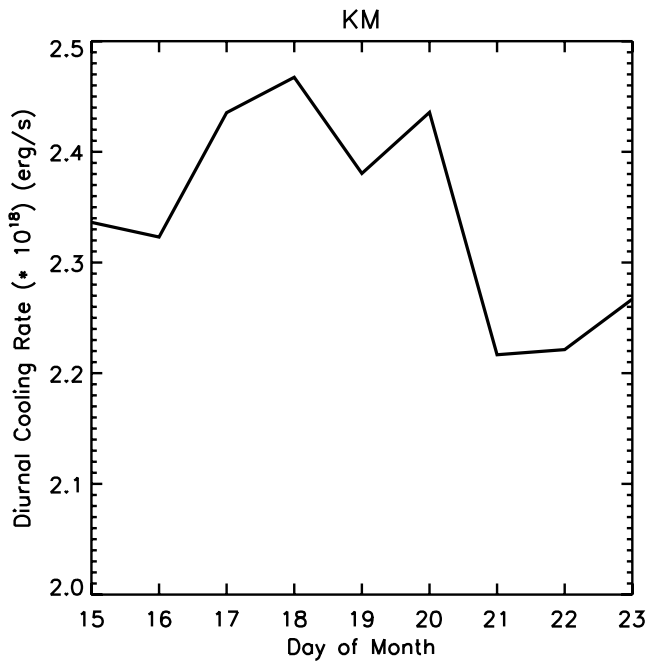

Figure 12. Thermospheric cooling rate (erg/s) due to heat conduction for each day 15 April through 23 April 2002 as computed by the ASPEN model.

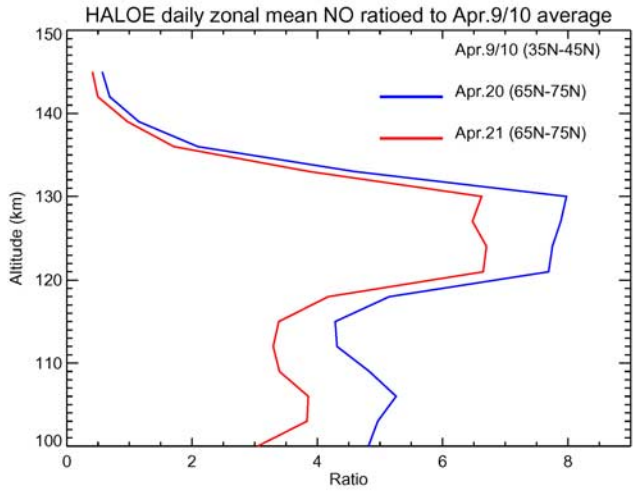

Figure 13a. HALOE daily zonal mean NO concentration from 20 April and 21 April relative to the NO measured on 9 and 10 April, at the indicated latitudes in the northern hemisphere.

(prior to the storm), in both northern (Figure 13a) and southern (Figure 13b) hemispheres. The HALOE data show increases in NO by factors of 2 to 8 depending on altitude. The HALOE data also suggest an enhancement in the northern hemisphere at 130 km that is a factor of 2 larger than in the southern hemisphere, consistent with the hemispheric asymmetry observed in the SABER zonal mean fluxes and power. The HALOE data strongly imply that changes in NO abundance are a major factor in the observed change in NO emission in the lower thermosphere.

[51] In order to assess the importance of temperature increases during the storm, we compute the ratio of the NO($\upsilon = 1$) emission rates using ASPEN model temperatures from day 104 (14 April) and 109 (19 April) assuming

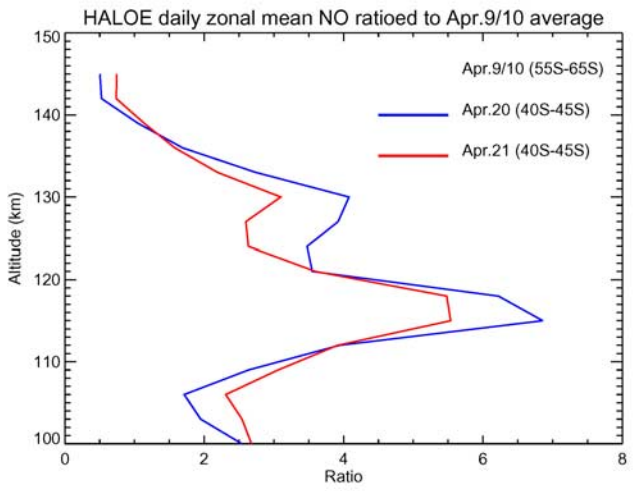

Figure 13b. HALOE daily zonal mean NO concentration from 20 April and 21 April relative to the NO measured on 9 and 10 April at the indicated latitudes in the northern hemisphere.

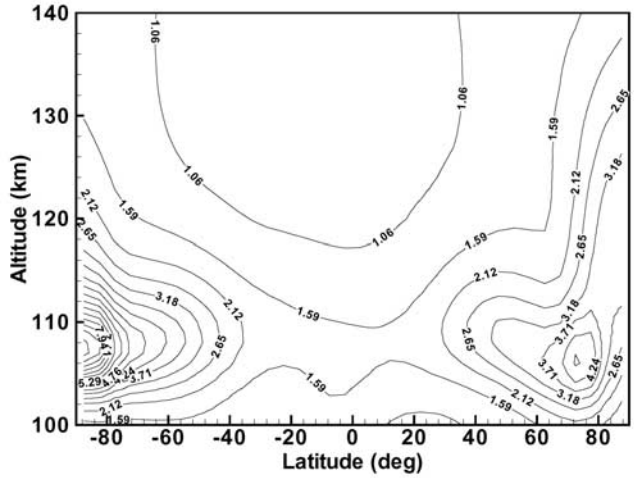

Figure 14a. Ratio of NO(1→0) volume emission rate computed with ASPEN model temperatures on 19 April (storm time) to the emission rate computed with ASPEN model temperatures on 14 April (quiet time) to illustrate the effect of temperature change on the NO emission rate, 100 km to 140 km altitude.

everything else is constant. The ratio R we evaluate is given by

$$R = \frac{\exp(-2700/T_{109})}{\exp(-2700/T_{104})}, \tag{15}$$

where T_{109} and T_{104} are the ASPEN temperatures on days 109 and 104, respectively. The value of 2700 is the energy (in K) of the NO(1-0) fundamental transition.

[52] Zonal mean values of R are shown for altitudes between 100 and 140 km in Figure 14a and between 140 km and 200 km in Figure 14b. Between 110 km and 120 km, increases in temperature alone could increase the NO emission by factors of 2 to 7. Between 120 and 140 km, increases in temperature could increase the emission by factors of 2 to 3. Above 140 km the temperature changes can increase the NO emission by as much as 50%. The effect of temperature on NO emission is the largest where the temperature is initially the lowest. These calculations suggest that temperature increases in the lower thermosphere can contribute significantly to the changes in NO emission while in the upper thermosphere the temperature changes should have much less of an effect.

[53] We consider now the two remaining potential mechanisms for NO emission enhancement, atomic oxygen increases and chemiluminescent emission increases. As shown above in section 5, changes in atomic oxygen predicted by ASPEN do not appear to be large (certainly not factors of 2 to 8 required to achieve the observed NO emission increase). Furthermore, chemiluminescent emission, even during storm time, is never larger than the emission from the fundamental 1–0 band of NO. We therefore infer that these two mechanisms are likely not major factors contributing to the observed NO emission increase.

[54] In summary, we conclude that in the lower thermosphere (below 140 km) a combination of NO concentration increases and temperature increases likely results in the

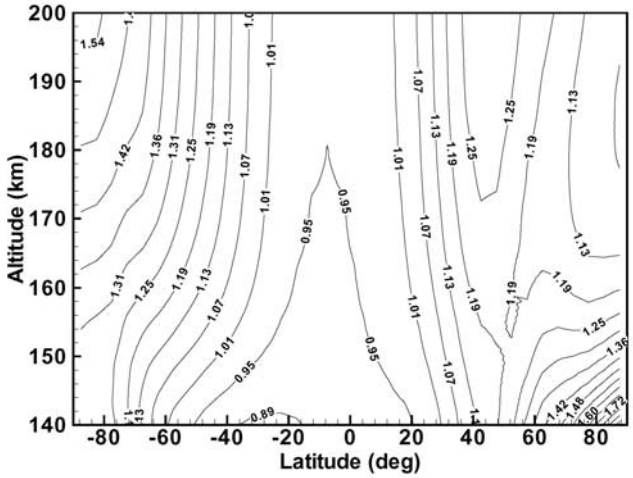

Figure 14b. Ratio of NO(1→0) volume emission rate computed with ASPEN model temperatures on 19 April (storm time) to the emission rate computed with ASPEN model temperatures on 14 April (quiet time) to illustrate the effect of temperature change on the NO emission rate, 140 km to 200 km altitude.

observed NO emission increase. In the middle and upper thermosphere (140 to 200 km) the observed increase in NO emission is likely due primarily to increases in NO abundance, with temperature increases secondary in importance. At all altitudes, changes in atomic oxygen and in chemiluminescent emission likely play much smaller roles than the other two mechanisms.

8. Summary and Recommendations for Future Work

[55] We have examined in detail the infrared radiative response of the thermosphere during the dramatic solar storm events of April 2002. On the basis of observations from the SABER instrument on the TIMED satellite, we find that the dominant infrared response is due to emission from the nitric oxide molecule at 5.3 μm. Carbon dioxide at 15 μm has a measurable but small response that is only a few percent of the nitric oxide and occurs over a much smaller range of altitudes. From simulations of the storm event with the ASPEN general circulation model and consideration of the physics of infrared radiation, we have shown the radiative response of atomic oxygen at 63 μm to be minimal. Computations of the rates of energy loss due to molecular heat conduction with the ASPEN model perhaps show a small increase in energy loss during the storm. Rates of energy loss from nitric oxide determined from the SABER measurements exceed 2000 K/day at the peak in the polar region near 175 km. Preliminary assessments suggest that enhancements in the NO emission are primarily due to increases in the NO abundance and in temperature. The hemispheric asymmetry in observed changes in the NO abundance is consistent with the SABER observations of enhanced radiative emission. These results confirm the ''natural thermostat'' role played by nitric oxide in mitigating the effects of intense solar disturbances on the atmosphere. All together, the radiative and conductive loss mechanisms account for about 30% of the amount of energy deposited in the upper atmosphere.

[56] This paper provides the basis for understanding the infrared response of the thermosphere to intense solar disturbances. Nevertheless, there are still several issues that should be addressed. Among these are (1) a complete accounting of the energy disposition in the mesosphere-thermosphere system relative to the estimated inputs of the total storm energy in the atmosphere, thereby closing the energy budget for the storm period; (2) a refinement of the relative importance of the various mechanisms responsible for the NO radiance enhancements; and (3) an assessment of possible feedbacks in the lower atmosphere. Solving these will significantly enhance our understanding of the response of the upper atmosphere and its potential coupling to the lower atmosphere to determine if these storm events alter the atmosphere for periods longer than the storm duration.

[57] **Acknowledgments.** MGM gratefully acknowledges the support of the NASA Science Mission Directorate for continued support of the SABER project and the TIMED mission and also the support of the Science Directorate at NASA Langley.

[58] Shadia Rifai Habbal thanks Ray Roble and Timothy J. Fuller-Rowell for their assistance in evaluating this paper.

References

Bates, D. R. (1951), The temperature of the upper atmosphere, *Proc. Phys. Soc., Ser. B*, *64*, 805–821.

Crowley, G., C. Freitas, A. Ridley, D. Winningham, R. G. Roble, and A. D. Richmond (1999), Next generation space weather specification and forecasting model, paper presented at Ionospheric Effects Symposium, Off. of Naval Res., Alexandria, Va.

Dothe, H., J. W. Duff, R. D. Sharma, and N. B. Wheeler (2002), A model of odd nitrogen in the aurorally dosed nighttime terrestrial thermosphere, *J. Geophys. Res.*, *107*(A7), 1071, doi:10.1029/2001JA000143.

Fink, E. H., H. Kruse, D. A. Ramsay, and M. Vervoloet (1986), An electric quadruple transition: the $b^1\Sigma_g^+ - a^1\Delta_g$ emission system of oxygen, *Can. J. Phys.*, *64*, 242–245.

Funke, B., and M. Lopez-Puertas (2000), Nonlocal thermodynamic equilibrium vibrational, rotational, and spin state distribution of NO(u = 0, 1, 2) under quiescent atmospheric conditions, *J. Geophys. Res.*, *105*(D4), 4409–4426.

Garcia, R. R., and S. Solomon (1994), A new numerical model of the middle atmosphere: 2. Ozone and related species, *J. Geophys. Res.*, *99*, 12,937–12,951.

Garcia, R. R., F. Stordal, S. Solomon, and J. Kiehl (1992), A new numerical model of the middle atmosphere: 1. Dynamical and transport of tropospheric source gases, *J. Geophys. Res.*, *97*, 12,967–12,991.

Gille, J. C., and F. House (1971), On the inversion of limb radiance measurements. I: temperature and thickness, *J. Atmos. Sci.*, *28*, 1427–1442.

Grossman, K. U., and K. Vollmann (1997), Thermal infrared measurements in the middle and upper atmosphere, *Adv. Space Res.*, *19*, 631–638.

Grossman, K. U., M. Kaufmann, and E. Gerstner (2000), A global measurement of lower thermosphere atomic oxygen densities, *Geophys. Res. Lett.*, *27*, 1387–1390.

Hagan, M. E., M. D. Burrage, J. M. Forbes, J. Hackney, W. J. Randel, and X. Zhang (1999), GSWM-98: Results for migrating solar tides, *J. Geophys. Res.*, *104*, 6813–6827.

Heelis, R. A., J. K. Lowell, and R. W. Spiro (1982), A model of the high latitude ionospheric convection pattern, *J. Geophys. Res.*, *87*, 6339.

Killeen, T. L., A. G. Burns, I. Azeem, S. Cochran, and R. G. Roble (1997), A theoretical analysis of the energy budget in the lower thermosphere, *J. Atmos. Sol. Terr. Phys.*, *59*, 675–689.

Kockarts, G. (1980), Nitric oxide cooling in the terrestrial thermosphere, *Geophys. Res. Lett.*, *7*, 137–140.

Kratz, D. P., M.-D. Chou, M.-H. Yan, and C.-H. Ho (1998), Minor trace gas radiative forcing calculations using the k distribution with one-parameter scaling, *J. Geophys. Res.*, *103*, 31,647–31,656.

Kratz, D. P., M. G. Mlynczak, C. J. Mertens, H. Brindley, L. L. Gordley, F. Martin-Torres, F. M. Miskolczi, and D. D. Turner (2005), An Intercomparison of far-infrared line-by-line radiative transfer models, *J. Quant. Spectrosc. Radiat. Transfer*, *90*(3–4), 323–341.

Lu, G., et al. (1998), Global energy deposition during the January 1997 magnetic cloud event, *J. Geophys. Res.*, *103*, 11,695–11,684.

Maeda, S., T. J. Fuller-Rowell, and D. S. Evans (1992), Heat budget of the thermosphere and temperature variations during the recovery phase of a geomagnetic storm, *J. Geophys. Res.*, *97*(A10), 14,947–14,957.

Mlynczak, M. G. (1995), Energetics of the middle atmosphere: Theory and observation requirements, *Adv. Space Res.*, *17*, 117–126.

Mlynczak, M. G. (1997), Energetics of the mesosphere and lower thermosphere and the SABER experiment, *Adv. Space Res.*, *20*, 1177–1183.

Mlynczak, M. G., et al. (2003), The natural thermostat of nitric oxide emission at 5.3 μm in the thermosphere observed during the solar storms of April 2002, *Geophys. Res. Lett.*, *30*(21), 2100, doi:10.1029/2003GL017693.

Mlynczak, M. G., F. J. Martin-Torres, D. G. Johnson, D. P. Kratz, W. A. Traub, and K. Jucks (2004), Observations of the O(^{3}P) fine structure line at 63 μm in the upper mesosphere and lower thermosphere, *J. Geophys. Res.*, *109*, A12306, doi:10.1029/2004JA010595.

Richmond, A. D., and Y. Kamide (1988), Mapping electrodynamic features of the high-latitude ionosphere from localized observations: Technique, *J. Geophys. Res.*, *93*, 5741–5759.

Roble, R. G. (1995), Energetics of the mesosphere and thermosphere, in *The Upper Mesosphere and Lower Thermosphere: A Review of Experiment and Theory*, *Geophys. Monogr. Ser.*, vol. 87, edited by R. M. Johnson and T. L. Killeen, pp. 1–21, AGU, Washington, D. C.

Roble, R. G., and E. C. Ridley (1987), An auroral model for the NCAR thermospheric general circulation model (TGCM), *Ann. Geophys.*, *5*, 369.

Roble, R. G., and E. C. Ridley (1994), Thermosphere-Ionosphere-Mesosphere-Electro Dynamics General Circulation Model (TIME-GCM): Equinox solar cycle minimum simulations (300–500 km), *Geophys. Res. Lett.*, *22*, 417.

Russell, J. M., M. G. Mlynczak, L. L. Gordley, J. Tansock, and R. Esplin (1999), An overview of the SABER experiment and preliminary calibration results, in *Proceedings of the 44th Annual Meeting, Denver, Colorado, July 18–23*, vol. 3756, pp. 277–288, SPIE, Bellingham, Wash.

Seppälä, A., P. T. Verronen, E. Kyrölä, S. Hassinen, and L. Backman (2004), Solar proton events of October–November 2003: Ozone depletion in the northern hemisphere polar winter as seen by GOMOS/Envisat, *Geophys. Res. Lett.*, *31*, L19107, doi:10.1029/2004GL021042.

Sharma, R. D., B. Zygelman, F. von Esse, and A. Dalgarno (1994), On the relationship between the population of the fine structure levels of the ground electronic state of atomic oxygen and the translational temperature, *Geophys. Res. Lett.*, *21*, 1731–1734.

Sharma, R. D., H. Dothe, and J. W. Duff (1998), Model of the 5.3 μm radiance form NO during the sunlit thermosphere, *J. Geophys. Res.*, *103*, 14,753–14,758.

Weimer, D. R. (1996), A flexible IMF dependent model of high-latitude electric potentials having "space weather" applications, *Geophys. Res. Lett.*, *23*, 2549–2553.

G. Crowley, Southwest Research Institute, 6220 Culebra Road, San Antonio, TX 78228-0510, USA.

B. Funke and M. Lopez-Puertas, Instituto de Astrofisica de Andalucia, Apdo. 3004, E-18080 Granada, Spain.

L. Gordley, G & A Technical Software, 11864 Canon Blvd., Suite 101, Newport News, VA 23606, USA.

J. Kozyra, University of Michigan, 2455 Hayward Street, Ann Arbor, MI 48109-2143, USA.

D. P. Kratz, C. Mertens, and M. G. Mlynczak, Science Directorate, NASA Langley Research Center, 21 Langley Blvd., Mail Stop 420, Hampton, VA 23681-0001, USA. (m.g.mlynczak@nasa.gov)

G. Lu, National Center for Atmospheric Research, P. O. Box 3000, Boulder, CO 80307-3000, USA.

F. J. Martin-Torres, AS & M Inc., Mail Stop 420, Hampton, VA 23681, USA.

L. Paxton, Johns Hopkins University Applied Physics Laboratory, Laurel, MD, USA.

R. Picard, R. Sharma, and J. Winick, Air Force Research Laboratory, 29 Randolph Road, Hanscom Air Force Base, MA 01731-3010, USA.

J. M. Russell III, Center for Atmospheric Sciences, Hampton University, Hampton, VA 23668, USA.